Studying the effect of high-viscosity material properties on print quality using laser-induced forward transfer

Hiroyuki Suhara* **and Jun Aoto**
RICOH Company, Ltd., Ebina-shi, Kanagawa, Japan

Abstract. A laser-induced forward transfer method that allows ejecting high-viscosity inks at a bubble ring pressure is presented. In this study, we clarify the transmittance and viscosity properties of donor materials that significantly affect the print quality. A nanosecond laser with a wavelength of 532 nm irradiates the donor in a ring shape. The relationship between the donor viscosity and print quality is analyzed, and optimal fluence is highly correlated with donor viscosity at a shear stress of 1000 Pa. A donor layer with a transmittance of 10% or less exhibits good droplet quality. When the transmittance of the donor layer is higher, backside fluence (BsF) will increase, resulting in mist and satellites. The BsF indicates that it is an important parameter for achieving droplet quality. These findings suggest that it is possible to develop a printing system using high-viscosity inks. [DOI: 10.1117/1.OE.61.10.104101]

Keywords: bubble ring; laser-induced forward transfer; transmittance; backside fluence; beam profile; print quality.

Paper 20220158G received Feb. 21, 2022; accepted for publication Sep. 23, 2022; published online Oct. 14, 2022.

1 Introduction

The printing of different inks using flexible and environmentally friendly approaches is an important requirement from the viewpoint of sustainable development goals. Digital printing technology is used in two- and three-dimensional (3D) printing and printed electronics. Inkjet printers,[1] thermal printers (TPs),[2] and electrophotography (EP) have been commercialized as digital printing technologies. These techniques have already gained high reliability and customer satisfaction. Inkjet printing systems have a high image quality and a good performance. This technique is incompatible with high-viscosity inks because of nozzle clogging. Therefore, it may be difficult to apply inkjet systems. TP and EP technologies can be used for high-viscosity materials; however, many restrictions with respect to receiver materials, including the sheet shape and heat resistance, limit their applications.

Recently, the laser-induced forward transfer (LIFT) method[3–6] has attracted attention for transferring solid and liquid materials to the receiver. As it is a nozzle-free process, this method can be used for high-viscosity inks. The LIFT also offers high flexibility in the range of receiver substrates. The LIFT method provides applications, such as 3D printing,[4] printed electronics for solar cells,[7] bioprinting,[8] and digital printing.[9]

The gap between the donor and receiver substrates should be kept at tens of micrometers or less to prevent low-quality prints in LIFT systems.[10–12] The gap should be 500 μm or more to increase the throughput for industrial applications. Furthermore, a gap of 1 mm or more should be used for printing uneven receivers and curved surface shapes. It has been reported that satellites or spray may generally occur when the gap is 100 μm or greater.[13] It has been reported that a high absorption film should be added between the transparent and the donor substrates to improve the droplet quality.[4,14–17]

Printing using high-viscosity inks with a long flight distance of more than 100 μm is a challenge for LIFT to surpass the already commercialized digital printing technology.

*Address all correspondence to Hiroyuki Suhara, suhara-h@jp.ricoh.com

We proposed a new LIFT method termed bubble ring (BR)-LIFT that allows the ejection of high-viscosity inks at a pressure of a ring-shaped vapor bubble.[18] We have succeeded in printing high-quality droplets even when the flight distance is 500 μm or more. A feature of BR-LIFT is that the droplet diameter does not depend on the pulse energy. The droplet diameter can be controlled by changing the ring diameter.[18]

The effects of viscoelastic properties or transmittance of donor materials have not been fully studied. The donor viscosity used in the experiment was performed under one condition.[18] The viscosity and important properties related to the LIFT phenomenon attributed to the interaction with the laser beam and greatly affect the flight morphology. Therefore, it is essential to understand how the different viscosities behave. However, most donor materials are non-Newtonian fluids (NNFs), and the viscosity of NNFs generally significantly changes based on a shear rate. Thus, it was unclear under what conditions viscosity is appropriate as an evaluation index to explain the LIFT phenomenon.

In this study, we report the relationship between donor viscosity and laser irradiation energy under high-quality droplet conditions using BR-LIFT and clarify an effective viscosity that is highly correlated with the fluence threshold. Next, we report the effect of inks with constant viscosity and different transmittance on print quality. Finally, we propose that backside fluence (BsF) is an important parameter for achieving droplet quality.

2 Experimental Setup

2.1 *BR-LIFT Method*

Figure 1 shows the BR-LIFT process. When a ring-shaped laser beam irradiates the donor layer from a transparent substrate side, a ring-shaped vapor bubble (hereinafter, BR) is generated in the boundary area between the transparent substrate and the frontside of the donor substrate, as shown in Fig. 1(a). In addition, low viscosity regions are formed near the BR in the boundary region and on the backside of the donor layer. This BR creates an inward pressure toward the axis. This phenomenon is consistent with the lateral flow observed in the central zone when two expanding bubbles are slightly separated.[19–21] Then, BR rapidly expands at an extremely high pressure, which drives the wrapped donor volume. The low-viscosity liquid envelops a high-viscosity liquid. Finally, the donor is ejected from the backside of the donor substrate and lands on the receiver, as shown in Fig. 1(b).

Figure 2 shows the BR-LIFT optical system. The light source used in the BR-LIFT system must exhibit a high-quality beam profile and high power. Thus, a nanosecond-pulsed fiber laser is used as the laser light source with a wavelength of 1064 nm. The maximum energy of the

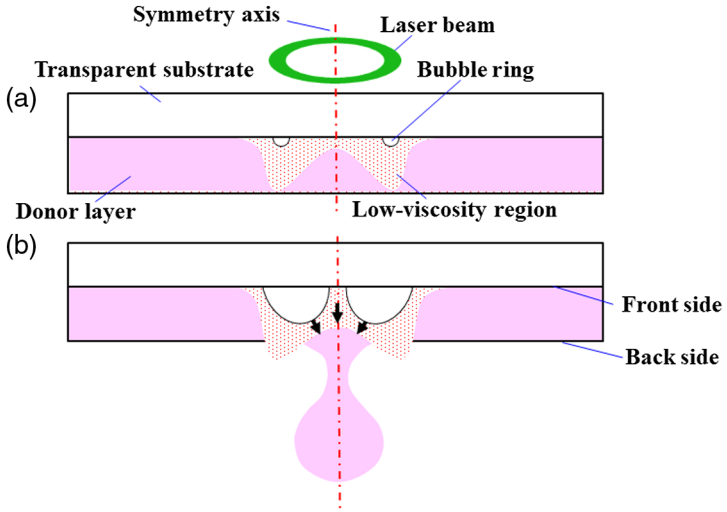

Fig. 1 BR–LIFT process: (a) the bubble ring is generated and (b) the donor is pushed out.

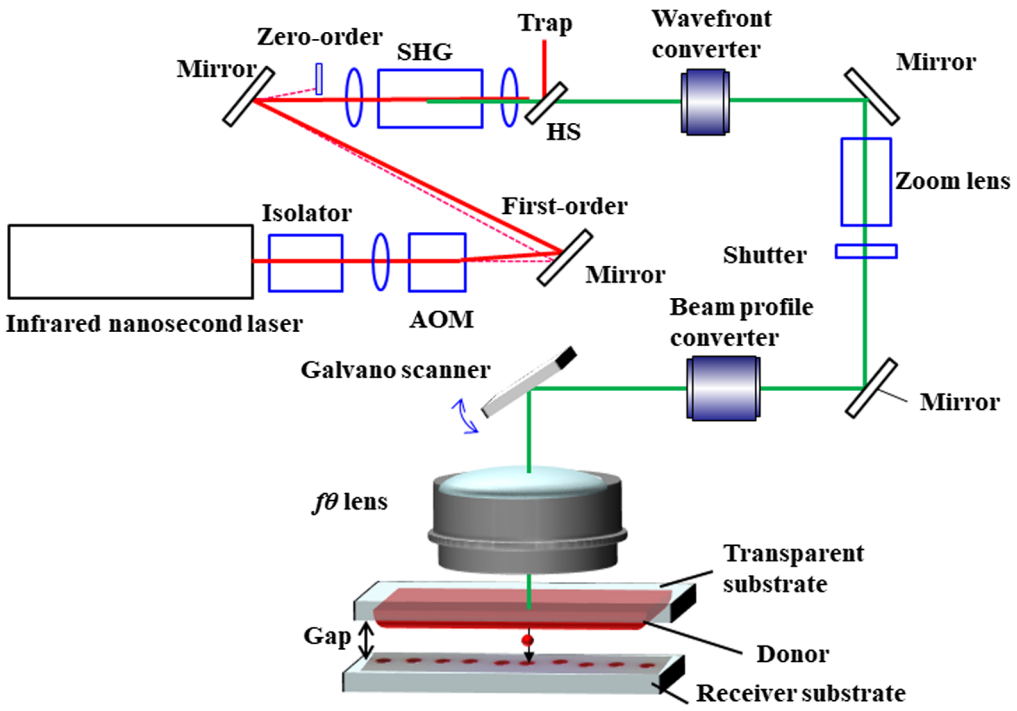

Fig. 2 Schematic diagram of the BR-LIFT system: AOM, acousto-optic modulator; SHG, second-harmonic generation element; HS, harmonic separator; ND, neutral density filter. SHG converts a wavelength of 1064 nm into that of 532 nm. The pulse duration is 8 ns.

pulsed laser is 0.2 mJ when the repetition rate is 50 kHz. The pulsed laser passes through a spatial isolator, quarter-wave plate, collimator lens, and acousto-optic modulator (AOM). The repetition rate of the pulsed laser is controlled using AOM. The laser then passes through a nonlinear optical crystal, inducing second-harmonic generation (SHG). The SHG converts a wavelength of 1064 nm into that of 532 nm.

Next, the laser beam passes through a wave front converter to make corrections, such as astigmatism.[22] Astigmatism is one of the most important factors that must be eliminated for a successful implementation of the BR-LIFT. The laser beam with a wavelength of 532 nm is converted into an annular beam by passing it through a beam converter. The beam converter consists of a reflective spatial light modulator (SLM) and a prism mirror.[18] The laser beam is reflected by the prism mirror and reaches the SLM. When the laser beam is reflected by the SLM, it is converted into the annular beam. The laser beam is then reflected again by the prism mirror and travels in the same direction as the incident beam.

Then, the laser beam passes through the mirror and other optics and is deflected using a galvano scanner. Finally, the laser beam focuses near the donor layer applied to the transparent substrate using the $f\theta$ lens. The incident beam diameter to the $f\theta$ lens is 3 mm, and the focal length of the $f\theta$ lens is 100 mm. The receiver is placed parallel to the donor layer and mounted on an adjustable stage. The annular beam maintains a constant profile at a distance of a few millimeters from the focal position. Figure 3 shows the annular beam with a ring diameter of 84 μm placed on the overfocus side by 0.5 mm from the focal position.

The light intensity distribution in the donor layer can be obtained using the Fresnel diffraction equation.[23] Figure 4 shows the light intensity distribution near the focal plane. The x_i–y_i plane represents the frontside of the donor. The Fresnel diffraction equation is represented as

$$u(x_i, y_i) = \frac{1}{j\lambda z_i} e^{ik\left[z_i + \frac{x_i^2 + y_i^2}{2z_i}\right]} \iint_{-\infty}^{+\infty} g(x_0, y_0) \exp\left\{jk\left(\frac{x_0^2 + y_0^2}{2z_i}\right)\right\} \exp\left[-j2\pi\left(\frac{x_0 x_i + y_0 y_i}{\lambda z_i}\right)\right] \mathrm{d}x_0\, \mathrm{d}y_0, \tag{1}$$

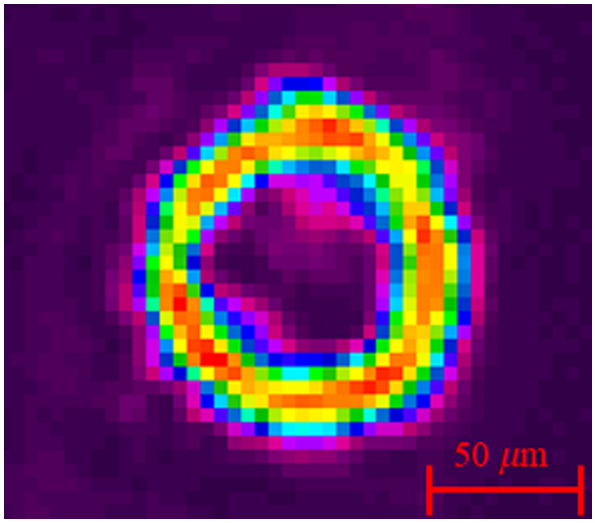

Fig. 3 Beam profile: the ring diameter was 84 μm.

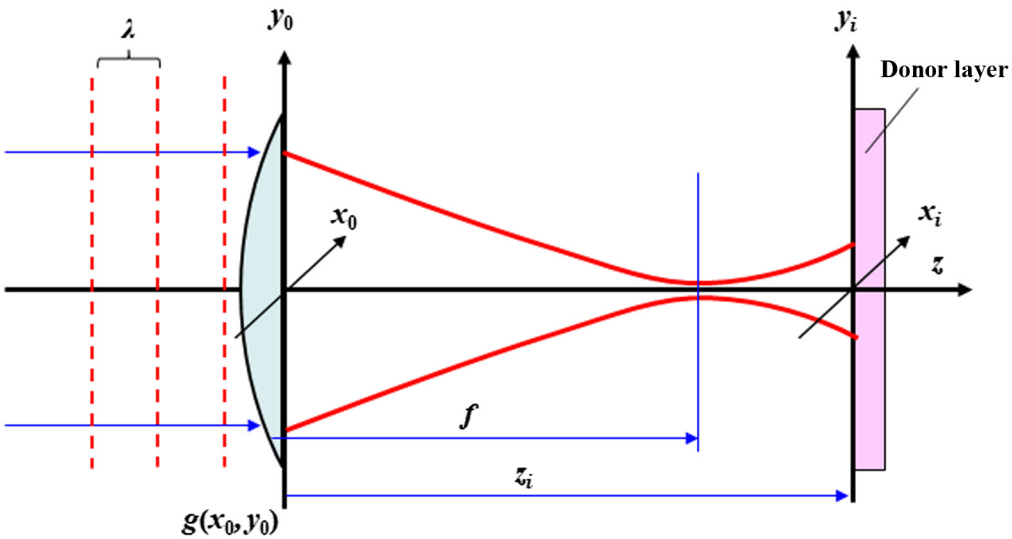

Fig. 4 Light intensity distribution near the focal plane.

where $g(x_0, y_0)$ is the complex amplitude of transmitted light and k is the wave number. When a parallel beam is incident on a lens whose diameter is assumed infinite, the complex amplitude of transmitted light on the x_0–y_0 plane is expressed using

$$g(x_0, y_0) \rightarrow g(x_0, y_0) \exp\left\{-jk\left(\frac{x_0^2 + y_0^2}{2f}\right) + j\varphi_0\right\}, \tag{2}$$

where f is the focal length. The φ_0 is insignificant for most of the analysis below and will be assumed as zero.[23] When we replace $g(x_0, y_0)$ in Eq. (1) with Eq. (2), we obtain

$$u(x_i, y_i) = \frac{1}{j\lambda z_i} e^{ik\left[z_i + \frac{x_i^2 + y_i^2}{2z_i}\right]} \iint_{-\infty}^{+\infty} g(x_0, y_0) \exp\left\{-jk\left(\frac{x_0^2 + y_0^2}{2f}\right) + jk\left(\frac{x_0^2 + y_0^2}{2z_i}\right)\right\} \exp k\left[-j2\pi\left(\frac{x_0 x_i + y_0 y_i}{\lambda z_i}\right)\right] \mathrm{d}x_0\, \mathrm{d}y_0. \tag{3}$$

Fraunhofer diffraction occurs when the x_i–y_i plane coincides with the focal length f, and the light intensity distribution is represented using the Fourier transform of $g(x_0, y_0)$. Next, the light intensity distribution near the focal plane is derived. When α is defined as

$$\alpha = \frac{k}{2}\left(-\frac{1}{f}+\frac{1}{z_i}\right), \tag{4}$$

substituting Eq. (4) into Eq. (3) yields

$$u(x_i, y_i) = \frac{1}{j\lambda z_i} e^{ik\left[z_i+\frac{x_i^2+y_i^2}{2z_i}\right]} \iint_{-\infty}^{+\infty} g(x_0, y_0) \exp\{-j\alpha(x_0^2+y_0^2)\} \exp[-j2\pi(f_x x_0 + f_y y_o)]\mathrm{d}x_0\,\mathrm{d}y_0. \tag{5}$$

In other words, the light intensity distribution near the focal plane agrees with the result of performing a Fourier transform by superimposing a quadratic function term to the phase term of $g(x_0, y_0)$. Thus, various patterns (e.g., changing ring diameters) can be created by changing the complex amplitude and focus position. In this optical system, SLM is used to generate an axicon wavefront,[24] a Bessel beam,[25] a Laguerre–Gaussian beam,[26] or superimposing them to generate a wavefront. The donor layer is arranged on the overfocus side by 0.5 mm from the focal position to carry out the experiment under the maximum peak power of the ring beam.

3 Experimental Results and Discussion

3.1 *Relationship Between Viscoelastic Properties and Fluence Threshold*

Clarifying the effect of the ink property is important to achieve high-quality printing. The donor viscosity is an important property involved in the interaction with light and significantly affects the droplet quality. The donor materials used in the experiment are NNFs and contain light-absorbing pigments and dyes. NNFs greatly vary in viscosity based on a shear rate.[27] It is unclear under which conditions viscosity is an appropriate as an evaluation index to explain the LIFT phenomenon.

Herein, we evaluated the correlation between irradiation energy and ink viscosity for each stress obtained in dynamic viscoelasticity measurements. In the viscoelasticity measurement, the storage elastic modulus (G') and loss elastic modulus (G'') can be obtained by applying stress to the liquid and detecting the strain and phase difference caused by the stress. The viscosity ($\eta = \sqrt{(G'^2 + G''^2)}/2\pi f$) is derived using G' and G''. The dynamic viscoelasticity was measured using a rheometer (HAAKE RheoStress600, Thermo Fisher Scientific).

Seven donor materials (types A to G) were fabricated using three ultraviolet (UV) curable inks (UV CORE type A [pigment red 57.1], UV CORE type A [pigment yellow 13], and BEST CURE UV flexo500 process red by T&K TOKA) and two viscosity modifiers (UV DG reducer and BEST CURE No. 2 UV contex by T&K TOKA).

Figure 5 shows the relationship between shear stress and viscosity measured using the rheometer. The seven donor materials are all NNFs. Types A and B inks are pseudoplastic fluids whose viscosity decreases by two orders of magnitude in the range from 1 to 1000 Pa. The viscosities of types C to G are adjusted to an almost constant viscosity that does not depend on a shear stress.

Table 1 shows the measurement results of different ink types and viscosities. Considering the four ink types A to D, at 1 Pa, types A and B exhibit approximately the same viscosity, and types C and D exhibit approximately the same viscosity. Additionally, at 1000 Pa, types A and D exhibit approximately the same viscosity, and types B and C exhibit approximately the same viscosity.

Figure 6 shows the relationship between laser fluence and the droplet diameter using type D donor materials as a typical sample. The ink donor substrate used in the experiment was 20 μm thick, and the transmittance of the donor layer was a few percentages or less. The transmittance was measured with a UV–Vis–NIR spectrophotometer UV3600 manufactured by Shimadzu. The receiver substrate was a photo paper, and the gap was set to 500 μm. One-shot exposure was performed at a scanning speed of 100 mm/s.

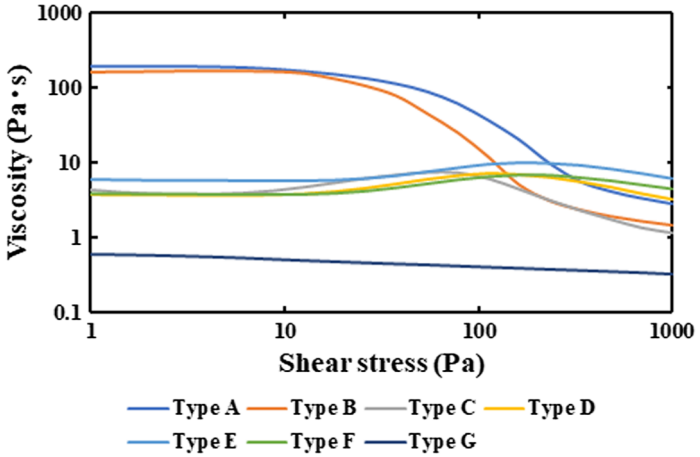

Fig. 5 Viscoelastic properties.

Table 1 Ink type and viscosity measurement results.

Ink type	Viscosity (1 Pa)	Viscosity (1000 Pa)
Type A	197.0	2.9
Type B	165.7	1.5
Type C	4.5	1.2
Type D	3.8	3.3
Type E	6.2	6.4
Type F	3.8	4.5
Type G	0.6	0.3

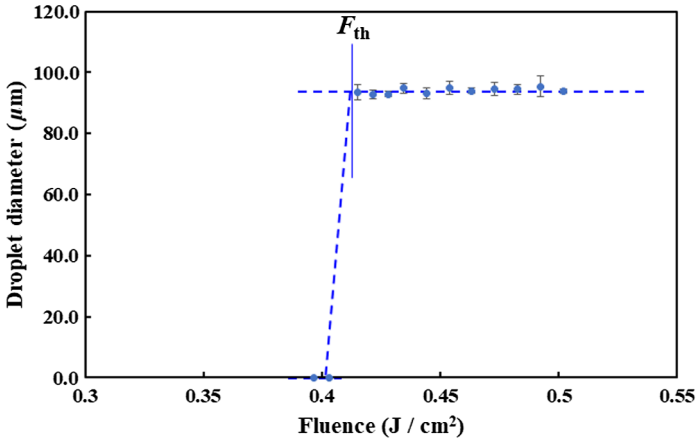

Fig. 6 Relationship between fluence and droplet diameter using type D donor materials.

Experimental results show that the diameter of the droplet remains constant regardless of the irradiation energy. Moreover, no droplets are generated when the fluence energy is reduced below the threshold. The fluence threshold is the optimal fluence for achieving high quality droplets. This fluence threshold is defined as F_{th}. In the result of Fig. 6, F_{th} is derived as $0.42\ \text{J/cm}^2$. The results show the same tendency in other donor materials.

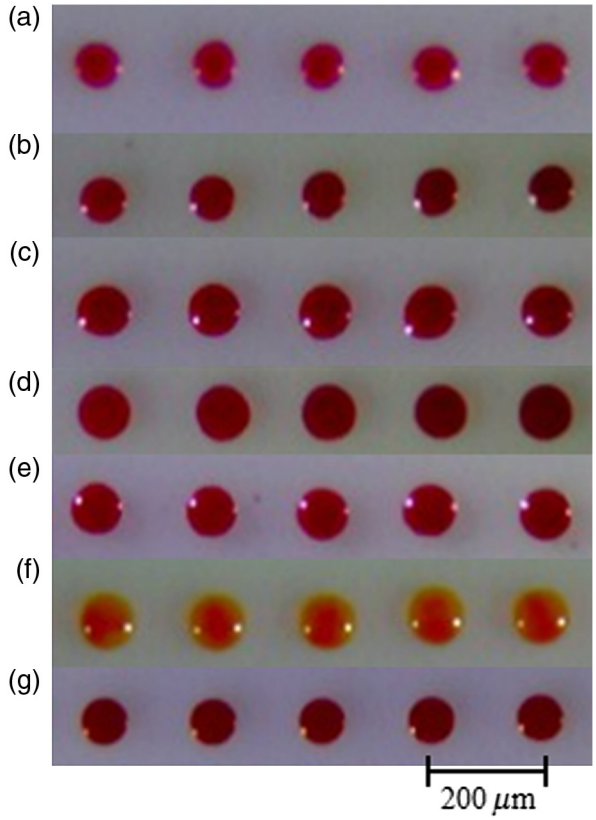

Fig. 7 Experimental results of landing droplets. (a)–(g) The experimental results of types A to G donor materials, respectively. Printing results obtained in a line at an interval of 200 μm using a galvano scanner. The gap was set to 500 μm. The bright spots on the left and right sides of droplets are artifacts owing to the illumination light from diagonally left and right.

Figure 7 shows the experimental results of landing droplets. Figures 7(a)–7(g) correspond to types A to G donor materials, respectively. Experiments were basically performed under the same conditions as in Fig. 6. BR-LIFT enables the printing of high-quality droplets for any materials listed in Table 1.

The experiment was performed by exposing a range of 10 mm at an interval of 200 μm. Multiple experiments were then performed while changing the exposure energy, and the minimum exposure energy required to print droplets was determined as the optimum exposure condition. Type F is different color from other types because it contains yellow ink in addition to magenta. The droplet diameters are slightly different depending on the different materials, but the reproducibility of the droplet diameters is high in the same donor materials. It was possible to print high-quality droplets for materials with a viscosity of 0.6 to 197 Pa·s under a shear stress of 1 Pa. These facts are reliable evidence of this method.

Figures 8(a)–8(d) show the relationship between the shear-stress viscosities of types A to G donor materials and the measured fluence thresholds to clarify the effective viscosity in the LIFT phenomenon. The dotted lines represent the logarithmic approximation lines. R^2 represents the correlation coefficient. F_{th} had a weak correlation with the viscosity at low shear stresses, i.e., 1 to 100 Pa. F_{th} had the highest correlation with the viscosity at 1000 Pa. It is presumed that the behavior of the ink when stress is applied is related to the flight state. The donor layer receives the gas pressure generated by the increasing heat in the high-viscosity ink owing to laser irradiation, as shown in Fig. 1. It is suggested that this ink was subjected to a stress equivalent to at least 1000 Pa in the flight process.

It is considered that the viscosity at 1000 Pa has a high correlation with F_{th} and accurately represents the material properties in the BR-LIFT system. Hereinafter, the viscosity at 1000 Pa is defined as the effective viscosity. Figure 8(d) shows that there is a logarithmically high correlation between an effective viscosity and F_{th}.

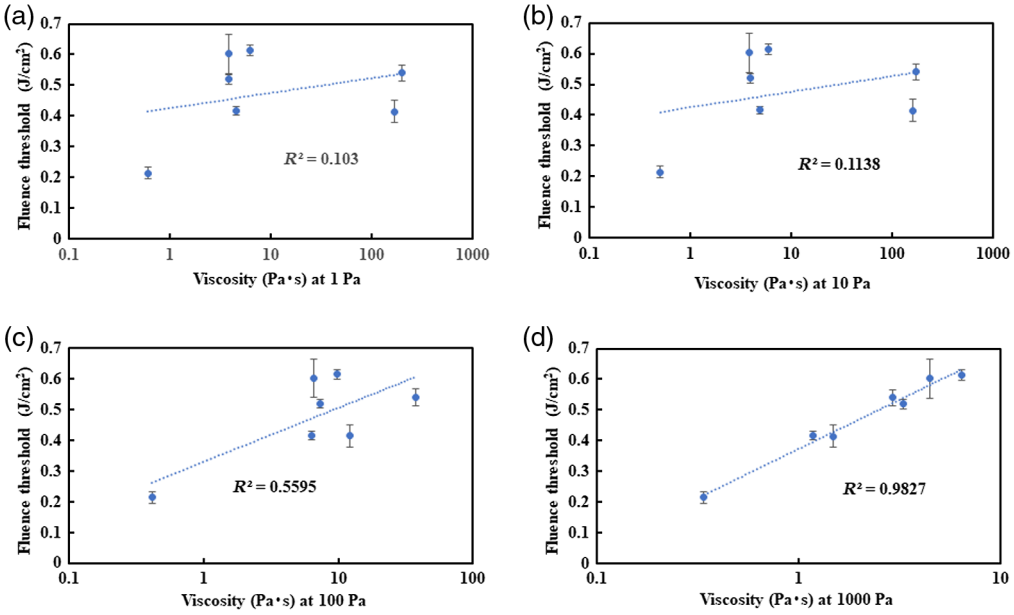

Fig. 8 Relationship between shear stress and fluence threshold.

3.2 *Relationship Between Donor Layer Transmittance and Droplet Quality*

The transmittance of a donor layer is known to depend on the droplet quality; however, this phenomenon is not yet fully understood quantitatively. For quantitative evaluation, a sample with a constant viscosity must be prepared. Therefore, we produced samples with different transmittances and a constant effective viscosity by changing the mixing ratio of two ink types with similar viscosities at 1000 Pa.

The donor material with the effective viscosity of ~4 Pa · s was used in the experiment. To fabricate the samples, a high-transmittance yellow ink (UV CORE type A yellow) and low-transmittance magenta ink (UV CORE type A red) were blended at ratios of 0.5%, 1%, 2%, and 5%. 5% magenta ink is the same prescription as type F in Table 1. All ink materials are obtained from T&K TOKA.

Table 2 shows the formulation of various inks. Four types of mixed inks were used. Multiple levels of film thickness were prepared. The film thickness was a value calculated from the coating weight and coating area, assuming that the specific gravity of ink was 1.1. Different experimental samples were prepared with a film thickness of 8 to 27 μm and transmittance of 4% to 51%. The transmittance was measured with the spectrophotometer UV3600.

Figure 9 shows the quality evaluation of landing droplets. The evaluation result "good" represents a state in which almost circular droplets are formed without satellites or with few satellites, as shown in Fig. 10(a). The evaluation result "not good" represents a state in which satellites and mists are generated in addition to droplets, as shown in Fig. 10(b). The judgment

Table 2 Formulation of various inks.

Sample ink type	Magenta ink weight (%)	Yellow ink weight (%)	Reducer weight (%)	Effective viscosity Pa·s)	Transmittance at 20 μm (%)
Type H	0.5	99.5	25	4.341	25
Type I	1	99	25	4.330	15
Type J	2	98	25	4.715	9
Type F	5	95	25.5	4.462	4

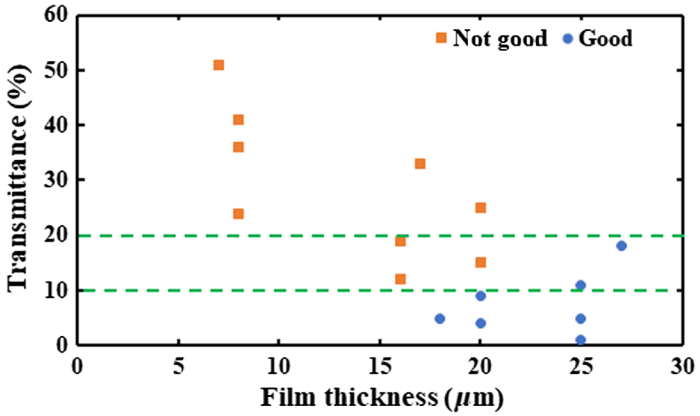

Fig. 9 Relationship between film thickness, transmittance, and droplet quality.

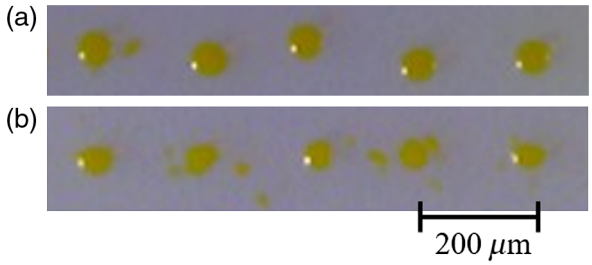

Fig. 10 Sample of the guideline for judgment criteria: (a) good sample and (b) not good sample. The judgment criteria are determined by the rate of satellite occurrence. If the number of satellites is one or less per dot, it is accepted. (a) Although there is the satellite, it is judged as good because it is a single satellite in five dots. (b) It is judged as not good because it is five dots and there are five or more satellites.

criteria were determined by the rate of satellite occurrence. If the number of satellites is 1 or less per dot, it is accepted.

The droplet quality under the condition of transmittance of 10% or less was good, as shown in Fig. 9. When the transmittance was 10% or more, the droplet quality gradually deteriorated. The droplet quality under the condition of transmittance of 10% or more and 20% or less is now mixed with good and not good. Furthermore, when the transmittance exceeded 20%, the droplet quality deteriorated overall.

The BsF was calculated to analyze the results of these experiments. We believe that BsF on the incident beam is an important parameter for achieving droplet quality. Moreover, the fluence of the ink surface on the incident side is called the frontside fluence (FsF) to distinguish between it and BsF. BsF does not affect reflectance. BsF is represented as

$$\mathrm{BsF} = \mathrm{FsF} \times T_{\mathrm{rans}}, \tag{6}$$

where T_{rans} is the transmittance. Incidentally, backside ablation[28,29] is generally a method of irradiating from the backside, which is different from the BsF used in this study.

Figure 11 shows the relationship between the transmittance of the donor layer and fluence. The FsF shows no correlation with transmittance, as shown in Fig. 11(a). In contrast, the BsF showed a high correlation with the transmittance regardless of good or not good, as shown in Fig. 11(b). These results indicate that BsF is an important parameter for achieving high-quality droplets.

The viscosity of the donor used in the experiment decreases as the temperature increases. The increasing temperature of the backside was calculated to understand the reason why the transmittance and BsF were highly correlated. The calculation of a backside temperature does not consider the effects of heat conduction. The donor expands and forms filaments in only ~5 μs

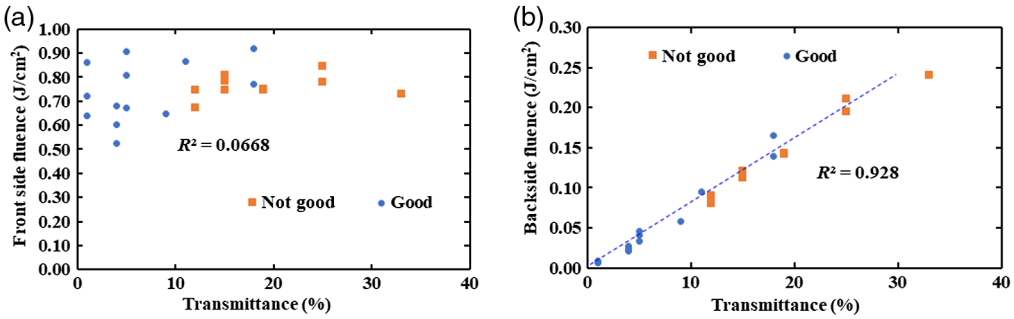

Fig. 11 Relationship between the transmittance of the donor layer and fluence: (a) front side fluence and (b) backside fluence.

after laser irradiation. When the laser irradiates the front surface of the donor layer with a film thickness of 20 μm and a thermal conductivity of 0.27 $\mathrm{W}/(\mathrm{m}\cdot\mathrm{K})$, the increasing temperature on the back surface after 5 μs is estimated to be only 1 deg or less. Thus, the effect of heat conduction can be ignored.

The increasing temperature of the liquid T_r is obtained as

$$T_r = Q/(v \cdot c \cdot \rho), \tag{7}$$

where v is the volume, c is the specific heat, and ρ is the density of the liquid. As representative values, $c = 1680$ $\mathrm{J}/(\mathrm{kg}\cdot\mathrm{K})$ and $\rho = 1174$ kg/m^3 were used. Note that Q is the amount of heat input, not the amount of irradiation. The required irradiation can be determined by considering the absorption rate or absorption coefficient of the donor material.

When the light intensity incident on the donor layer is I_0, the light intensity I on the backside of the donor layer is defined as $I = I_0 \exp(-\alpha t)$ using Beer–Lambert's law. Here, α is the absorption coefficient, t is the film thickness, and I/I_0 is the absorption rate at film thickness t. This implies that the amount of heat input differs in the depth direction and that the increasing temperature varies. Figure 12 shows the relationship between the transmittance of the donor layer and the increasing temperature T_r. T_r is obtained by substituting Q derived from Eq. (6) and Beer–Lambert's law into Eq. (7).

The experimental results were divided into two categories at an increasing temperature of ~55 K (hereinafter, T_b), as shown in Fig. 12. As accurately measuring the temperature is difficult, T_b is just a reference value. It was revealed that the temperature of the backside affects the high-quality printing.

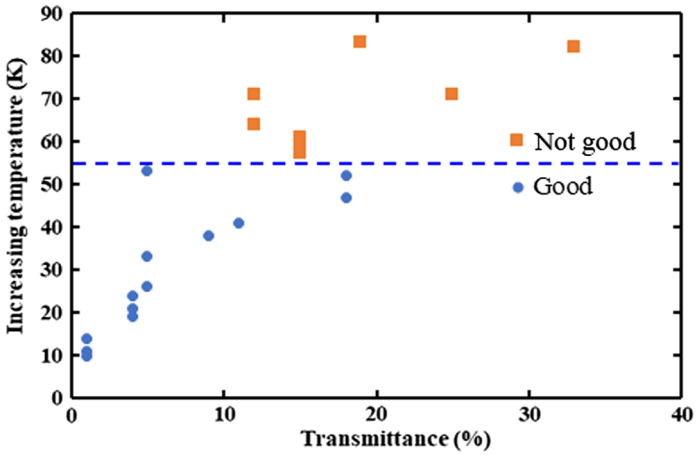

Fig. 12 Relationship between the transmittance of the donor layer and the increasing temperature on the backside.

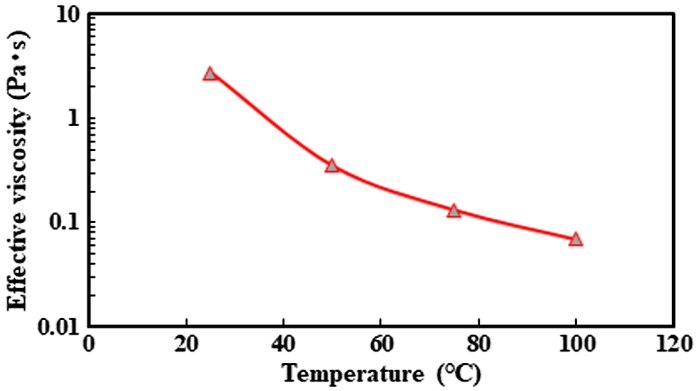

Fig. 13 Temperature dependence on effective viscosity.

We consider the causal relationship between the increasing temperature on the backside of the donor layer and the generation of satellites and mist. The temperature of the donor layer increases owing to heat accumulation under laser irradiation.

When the donor material complies with Andrade's equation, the viscosity of the donor layer decreases because of the temperature increase associated with laser irradiation.[30] Andrade's equation has been proposed to describe the temperature dependence on the viscosity

$$\eta = B \exp\left(\frac{E}{RT}\right), \tag{8}$$

where η is the dynamic viscosity, T is the absolute temperature, R is the Boltzmann constant, B is the proportional constant, and E is the activation energy. Figure 13 shows the measurement results of the temperature and effective viscosity of high-viscosity ink used in the experiment. The temperature was measured by a thermometer mounted on the rheometer RheoStress600.

The viscosity of high-viscosity ink shown in Fig. 13 decreases as temperature increases, i.e., the ink viscosity decreases to 0.13 Pa at a temperature of 75°C. When the temperature increases above T_b, the ink viscosity decreases, and mist is likely to form under low-energy conditions. In other words, if the transmittance is excessively high, the temperature of the backside of the donor layer becomes excessively high and owing to a decrease in the viscosity, mists will be easily generated. For a high-transmittance material, BsF can be reduced by increasing the film thickness. Thus, the film thickness must preferably be set according to the absorption characteristics of the donor material.

It is estimated that the donor material partially begins to undergo thermal pyrolysis at 200°C and reaches thermal pyrolysis completion at 500°C or higher. BR is caused by the gas pressure generated by the increase in heat in the high-viscosity ink associated with laser irradiation.[4] It can be estimated that when the frontside temperature rises by 500 K due to laser irradiation, the backside temperature with a transmittance of 10% rises by 50 K. In the case of a donor layer with a transmittance of 10% or less, BR-LIFT experiment can be carried out under the favorable conditions of T_b or less. In contrast, when the transmittance exceeds 10%, the increasing temperature of the backside becomes higher than T_b, resulting mist generation. Alternatively, if the experiment is conducted under the energy condition of T_b or less, BR cannot be formed on the frontside due to insufficient energy. Therefore, the conditions for achieving both frontside and backside temperatures of the donor layer are set within a limited range.

3.3 *Discussion*

In this study, we clarified that a shear stress of 1000 Pa should be set as the effective viscosity as an evaluation index for explaining the LIFT phenomenon. We also clarified that BsF for a transparent material is an important parameter that affects print quality. Table 3 shows a comparison between BR-LIFT and typical LIFT.

Table 3 Method comparison.

	Beam profile	Gap	Viscosity parameter	Fluence parameter
BR-LIFT	Annular	500 μm or more	1000 Pa	BsF and FsF
Typical LIFT	Gaussian	Tens of micrometers	Static	FsF

These findings suggest that BR-LIFT can be used in various practical applications. Specifically, a thick coating layer will be feasible for printed electronics and digital deposition by adopting a high-viscosity material. Digital full-color printing utilizes cyan, magenta, yellow, and black inks. By adjusting the film thickness to optimize the BsF, it should be possible to print any color with high quality, even if the transmission of each ink is different.

BR-LIFT can contribute to the mass production process due to the advantage of its long flight distance. Using a diffractive optical element instead of an SLM, a simple and low-cost optical system can be developed. The donor material is limited to an effective viscosity of 6 Pa·s or less. If BR-LIFT can be applied with effective viscosity materials of tens of Pa·s, screen printing ink and letterpress ink can be used. Thus, our proposed method should be a promising alternative to the conventional method.

4 Conclusions

In this study, we clarified the properties of the donor material required for high-viscosity liquid printing using BR-LIFT. The relationship between the donor viscoelasticity and irradiation energy is analyzed at a shear stress range of 1 to 1000 Pa. Consequently, at a shear stress of 1000 Pa, the ink viscosity exhibits a high correlation with the fluence threshold and accurately represents the material properties in the BR-LIFT system. The viscosity at 1000 Pa is suitable as the effective viscosity.

According to the experimental results on donor materials with constant viscosity and different transmittance, the donor layer with a transmittance of 10% or less exhibits good droplet quality. When the transmittance was 10% or more, the droplet quality gradually deteriorates. The transmittance has a great effect on the BsF. When the transmittance is higher, BsF will increase, thereby resulting in mist and satellites. The BsF indicates that it is an important parameter that affects print quality.

These findings show that BR-LIFT can be used in various practical applications, including digital deposition, security printing, bioprinting, and printed electronics. BR-LIFT can contribute to optimization in the practical stage and mass production process.

Acknowledgments

The authors would like to thank Yoshio Wada for his valuable advice on the laser system and Keiichi Kato for his assistance with the laser prototype. The authors declare no conflicts of interest.

References

1. H. J. J. Staat et al., "Ultrafast imaging method to measure surface tension and viscosity of inkjet-printed droplets in flight," *Exp. Fluids* **58**, 2 (2017).
2. D. G. Foster, "Thermal printing for digital output," in *Int. Symp. Technol. Digit. Photo Fulfillment*, pp. 68–69 (2009).
3. P. Delaporte and A. P. Alloncle, "Laser-induced forward transfer: a high resolution additive manufacturing technology," *Opt. Laser Technol.* **78**, 33–41 (2016).
4. P. Serra and A. Piqué, "Laser-induced forward transfer: fundamentals and applications," *Adv. Mater. Technol.* **4**(1), 1800099 (2019).

5. I. Theodorakos et al., "Laser-induced forward transfer of high viscous, non-Newtonian silver nanoparticle inks: jet dynamics and temporal evolution of the printed droplet study," *Adv. Eng. Mater.* **21**(10), 1900605 (2019).
6. A. Piqué et al., "Laser decal transfer of electronic materials with thin film characteristics," *Proc. SPIE* **6879**, 687911 (2008).
7. Y. Chen et al., "Laser induced forward transfer of high viscosity silver paste for new metallization methods in photovoltaic and flexible electronics industry," *Phys. Proc.* **83**, 204–210 (2016).
8. C. B. Arnold, P. Serra, and A. Piqué, "Laser direct-write techniques for printing of complex materials," *MRS Bull.* **32**, 23–31 (2007).
9. G. Hennig et al., "Lasersonic® LIFT process for large area digital printing," *J. Laser Micro Nanoeng.* **7**, 299–305 (2012).
10. J. Mikšys, G. Arutinov, and G. R. B. E. Römer, "Pico- to nanosecond pulsed laser-induced forward transfer (LIFT) of silver nanoparticle inks: a comparative study," *Appl. Phys. A Mater. Sci. Process.* **125**(12), 814 (2019).
11. D. Munoz-Martin et al., "Laser-induced forward transfer of high-viscosity silver pastes," *Appl. Surf. Sci.* **366**, 389–396 (2016).
12. V. Dinca et al., "Patterning parameters for biomolecules microarrays constructed with nanosecond and femtosecond UV lasers," *Thin Solid Films* **516**, 6504–6511 (2008).
13. L. Rapp et al., "Pulsed-laser printing of silver nanoparticles ink: control of morphological properties," *Opt. Express* **19**, 21563 (2011).
14. E. Turkoz, L. Deike, and C. B. Arnold, "Comparison of jets from Newtonian and non-Newtonian fluids induced by blister-actuated laser-induced forward transfer (BA-LIFT)," *Appl. Phys. A Mater. Sci. Process.* **123**(10), 652 (2017).
15. E. Turkoz et al., "Impulsively induced jets from viscoelastic films for high-resolution printing," *Phys. Rev. Lett.* **120**(7), 074501 (2018).
16. R. Pohl, *Laser-induced Forward Transfer of Pure Metals*, University of Twente (2015).
17. M. Zenou and Z. Kotler, "Printing of metallic 3D micro-objects by laser induced forward transfer," *Opt. Express* **24**, 1431 (2016).
18. H. Suhara, J. Aoto, and M. Iwata, "Printing method for long flight distance by laser-induced forward transfer," *J. Laser Micro Nanoeng.* **15**, 143–149 (2020).
19. A. Patrascioiu et al., "Interaction between jets during laser-induced forward transfer," *Appl. Phys. Lett.* **105**(1), 014101 (2014).
20. A. Patrascioiu et al., "Laser-generated liquid microjets: correlation between bubble dynamics and liquid ejection," *Microfluid. Nanofluid.* **16**, 55–63 (2014).
21. Y. L. Liu et al., "The motion of a 3D toroidal bubble and its interaction with a free surface near an inclined boundary," *Phys. Fluids* **28**(12), 122101 (2016).
22. H. Suhara, A. Tamura, and T. Nishio, "Beam shaping method using beam size and wavefront converters in ultrashort-pulse laser processing," in *Proc. LPM 2018*, pp. 18–63 (2018).
23. K. Iizuka, *Engineering Optics*, 4th ed., Springer International Publishing (2019).
24. M. Rioux, R. Tremblay, and P. A. Bélanger, "Linear, annular, and radial focusing with axicons and applications to laser machining," *Appl. Opt.* **17**, 1532 (1978).
25. N. Chattrapiban et al., "Generation of nondiffracting Bessel beams by use of a spatial light modulator" (2003).
26. R. Nakamura et al., "Optical vortex-induced forward mass transfer: manifestation of helical trajectory of optical vortex," *Opt. Express* **27**, 38019 (2019).
27. A. Kalaitzis et al., "Jetting dynamics of Newtonian and non-Newtonian fluids via laser-induced forward transfer: experimental and simulation studies," *Appl. Surf. Sci.* **465**, 136–142 (2019).
28. K. X. Zhang et al., "Fast fabrication of fishnet optical metamaterial based on femtosecond laser induced stress break technique," *Nanomaterials* **11**(3), 742 (2021).
29. R. Fardel et al., "Shadowgraphy investigation of laser-induced forward transfer: front side and back side ablation of the triazene polymer sacrificial layer," *Appl. Surf. Sci.* **255**, 5430–5434 (2009).
30. O. O. Okoturo and T. J. VanderNoot, "Temperature dependence of viscosity for room temperature ionic liquids," *J. Electroanal. Chem.* **568**, 167–181 (2004).

Hiroyuki Suhara received his BS and MS degrees in science and engineering from Waseda University in 1987 and 1989, respectively, and his PhD in fundamental science and engineering from Waseda University in 2015. He has worked for Ricoh Advanced Technology R&D Division. His research interests include laser beam shaping technology, optical interferometry, and applied charged particle optics.

Jun Aoto received his BS degree from First Cluster of Colleges of University of Tsukuba in 1988. He has worked for Ricoh Advanced Technology R&D Division. His research interests include material processing and material formulation design.